J. Biochem. 2009;146(4)535–540
doi:10.1093/jb/mvp098

Crystal Structure of Hypothetical Protein HP0062 (O24902_HELPY) from *Helicobacter pylori* at 1.65 Å Resolution

Sun-Bok Jang[1,*], Ae-Ran Kwon[2,*], Woo-Sung Son[1], Sung Jean Park[1] and Bong-Jin Lee[1,†]

[1]Research Institute of Pharmaceutical Sciences, College of Pharmacy, Seoul National University, San 56-1, Shillim-Dong, Kwanak-Gu, Seoul 151-742, Korea; and [2]Department of Herbal Skin Care, College of Herbal Bio-Industry, Daegu Haany University, 290, Yugok-Dong, Gyeongsan-Si, Gyeongsangbuk-Do, 712-715, Korea

Received May 8, 2009; accepted June 16, 2009; published online June 29, 2009

The HP0062 gene encodes a small acidic protein of 86 amino acids with a theoretical pI of 4.6. The crystal structure of hypothetical protein HP0062 from *Helicobacter pylori* has been determined at 1.65 Å by molecular-replacement method. The crystallographic asymmetric unit contains dimer, in which HP0062 monomer folds into a helix–hairpin–helix structure. The two protomers are primarily held together by extensive hydrophobic interactions in an antiparallel arrangement, forming a four helix bundle. Aromatic residues located at *a* or *g* position in the heptad leucine zipper are not major contributor required for HP0062 dimerization but important for the thermostability of this protein.

Key words: dimerization interface, *Helicobacter pylori*, helix–hairpin–helix structure, HP0062, leucine-zipper.

Abbreviations: ADSC, Area Detector Systems Corporation; CCD, Charge-Coupled Device; CD, Circular Dichroism; NCS, Non-Crystallographic Symmetry; ORFs, Open Reading Frames; RMSD, Root Mean Square Deviation; SDS-PAGE, SDS-polyacrylamide gel electrophoresis; TTS, Type III Secretion.

Helicobacter pylori is a Gram-negative, pathogenic bacterium that infects half of the world's population and is responsible for the majority of the cases of gastric and duodenal ulcers (*1*). It is the only organism that is uniquely adapted to survive in the low pH conditions and can establish a permanent infection of the human stomach. In the most severe cases, long-term infection can lead to gastric cancer (*2*).

Currently, three complete genome sequences of *H. pylori* strain 26695, J99 and HPAG1 have been determined (*3–5*). In the chromosome of strain 26695, 1,590 open reading frames (ORFs) were identified. Among them, 499 ORFs are annotated as 'hypothetical proteins' whose function and 3D structures have never been identified.

As the part of our structural genomics effort on *H. pylori*, we have determined the 3D structure of hypothetical protein HP0062 (O24902_HELPY) at 1.65 Å resolution. The HP0062 gene encodes a small acidic protein of 86 amino acids with a theoretical pI of 4.6. Primary structure of HP0062 displays a modified leucine zipper, in which additional aromatic residues are located at *a* or *g* position in the leucine zipper. In order to verify the role of the aromatic residues (F14, F21, F36) in the structural integrity of HP0062, we made triple mutant (F14, 21, 36A) and compared thermostabilities of HP0062 wild-type and its triple mutant protein. We also speculated the biological role of HP0062 based on the gene characteristics and 3D structural comparisons.

MATERIALS AND METHODS

Cloning, expression and purification—The predicted ORF of HP0062 was amplified from *H. pylori* strain 26695 genomic DNA using standard PCR methods and ligated into a pET-21a(+) expression vector (Novagen, Darmstadt, Germany). The resulting construct contains eight non-native residues at the C-terminus (LEHHHHHH) that facilitate protein purification. The accuracy of the cloning was confirmed by DNA sequencing. The resulting expression plasmid was then transformed into *Escherichia coli* BL21(DE3) (Novagen). Cells were grown at 37°C until $A_{600} = 0.6$ and expression was induced by the addition of isopropyl-β-D-thiogalactopyranoside to a final concentration of 0.5 mM. After an additional 4 h of growth at 37°C, cells were harvested by centrifugation and resuspended in 50 mM Tris–HCl, pH 7.5 and 0.5 M NaCl buffer. Cells were lysed by sonication at 4°C and the supernatant was loaded to Ni^{2+}-NTA column (Qiagen, Turnberry Lane Valencia, Ca, USA; 3 ml of resin per liter of cell culture) previously equilibrated with the same buffer. The column was washed extensively with wash buffer (50 mM Tris–HCl, pH 7.5, 0.5 M NaCl and 50 mM imidazole); then the bound protein was eluted with elution buffer (50 mM Tris–HCl, pH 7.5, 0.5 M NaCl and 500 mM imidazole) until there was no detectable absorbance at 280 nm in the eluant. Fractions containing protein were concentrated to ~2 ml and applied to a Superdex-75 (Pharmacia, Uppsala, Sweden) column that had been equilibrated

*These two authors contributed equally to this work.
†To whom correspondence should be addressed.
Tel: +82-2-880-7869, Fax: +82-2-872-3632,
E-mail: lbj@nmr.snu.ac.kr

with the final buffer (50 mM Tris–HCl, pH 7.5 and 0.15 M NaCl). Purified protein was judged to be >95% pure by SDS–PAGE. The triple mutant of $HP0062_{F14,21,36A}$, in which the three phenylalanine residues (F14, F21, F36) were substituted with alanine, was constructed by site-directed mutagenesis using the Quick Change Site-Directed Mutagenesis kit (Stratagene, La Jolla, CA, USA) according to the manufacturer's instructions. The mutation was confirmed by DNA sequencing. Protein expression and purification were performed as previously described for the wild-type HP0062.

Crystallization and Data Collection—HP0062 protein was concentrated to 12–15 mg/ml in 50 mM Tris–HCl, pH 7.5, 0.15 M NaCl and crystals were grown using the hanging-drop vapour diffusion method at 293 K. Crystals were obtained after several days by mixing 1 μl of protein solution and 1 μl of precipitant solution (4–6% PEG3350, 100 mM citrate, pH 4.5) and equilibrating against 1 ml reservoir of precipitant solution. For crystal freezing, crystals were transferred to a cryoprotecting solution containing 8% PEG3350, 100 mM citrate, pH 4.5, 30% glycerol within a minute in several steps and flash-frozen in a stream of nitrogen gas at ~100 K. Crystallographic data were collected on the beamline 6C of the Pohang Light Source (PLS), South Korea, using an ADSC Quantum 210 CCD detector, with radiation of wavelength $\lambda = 1.23985$ Å. The data set was processed and scaled with HKL2000 (*6*). The crystals are orthorhombic in space group $P2_12_12_1$. The data collection and processing statistics are summarized in Table 1.

Structure Determination and Refinement—A test set constituting 5% of the scattering amplitudes was selected for cross-validation. The structure of HP0062 was determined by molecular replacement using the program AMoRe (*7*) with the previously known structure of HP0062 as a search model (PDB ID: 2gts). In particular, molecular replacement searches affected with using monomer which is generated by symmetry operation were successful. Rigid body refinement followed by torsional-simulated annealing and group B factor refinement reduced the R-factors to $R_{cryst} = 0.319$, $R_{free} = 0.323$. The initial model was subjected to iterative cycles of manual model building with Coot (*8*), and crystallographic refinement by CNS (*9*) and Refmac 5.0 (*10*) in CCP4. Non-crystallographic symmetry (NCS) was implemented over two monomers with the restraint weight of 300 kcal/mole/Å^2. Solvent molecules became apparent in the later stages of refinement and were added into the model. Two final rounds of TLS restrained refinement (without any NCS restraints) were carried out using Refmac 5.0 (*11*). Further refinement was pursued until no further decrease of the R_{free} was observed ($R_{cryst} = 0.186$, $R_{free} = 0.225$).

The refinement statistics are summarized in Table 1. Overall quality of the model is excellent with 100% residues in the allowed regions of Ramachandran plot. Coordinates and experimental structure factors of the HP0062 structure have been deposited in the Protein Data Bank with accession code ID 3fx7.

Circular Dichroism—Circular dichroism (CD) spectra were collected on a J-715 Spectropolarimeter (Jasco, Hachioji, Japan) equipped with a peltier temperature control system (Model PTC-348WI). All measurements were performed with purified HP0062 samples (0.2 mg/ml) in 50 mM sodium phosphate buffer (pH 6.8). Samples were scanned three times with a bandwidth of 1 nm and a response time of 2 s from 190 to 250 nm at a rate of 50 nm/min. Thermal denaturation curves were obtained by monitoring the change in molar ellipticity at 222 nm at a scan rate of 1°C/min by increasing and decreasing the temperature in the range of 20–100°C. By monitoring changes in secondary structure content, apparent transition temperature (T_{app}) values were estimated by fitting the data using the five-parameter sigmoid function from curve-fitting program Sigmaplot, followed by determining the inflection point by numerical differentiation of the curves with Origin 8.

Table 1. **Crystallographic data collection and refinement statistics.**

Data collection	
Beam line	BL-6C (PLS)
Wavelength (Å)	1.23985
Resolution range (Å)	40.0–1.65 (1.71–1.65)[a]
Space group	$P2_12_12_1$
Unit cell parameters (Å)	$a = 39.30$, $b = 51.90$, $c = 83.31$
Observations (total/unique)	264,154/20,637
Completeness (%)	97.1 (95.1)
Redundancy	12.8 (12.6)
R_{sym}[b]	4.9 (24.8)
I/σ	59.3 (11.0)
Refinement	
Resolution range (Å)	40.0–1.65 (1.69–1.65)
R_{work}[c] (%)	18.6
R_{free}[c] (%)	22.5
Protein atoms	1,554
Water molecules	100
Average *B*-value (Å^2)	15.3
RMSD from ideal geometry	
Bond length (Å)	0.010
Angles (in degrees)	1.125
Ramachandran analysis (%)	
Most favoured region	97.6
Additional allowed region	2.4
Generously allowed region	0.0
Disallowed region	0.0

[a]Numbers in parentheses indicate the statistics for the last resolution shell. [b]$R_{sym} = \sum|I_{hkl} - \langle I_{hkl}\rangle|/\sum\langle I_{hkl}\rangle$, where I_{hkl}, single value of measured intensity of *hkl* reflection; and $\langle I_{hkl}\rangle$, mean of all measured value intensity of *hkl* reflection. [c]$R_{work} = \sum|F_{obs} - F_{calc}|/\sum F_{obs}$, where F_{obs}, observed structure factor amplitude; and F_{calc}, structure factor calculated from model. R_{free} is computed in the same manner as R_{work}, using the test set of reflections.

RESULTS AND DISCUSSION

Overall Structure of HP0062 and Dimeric State—The HP0062 monomer folds into a hairpin structure, in which two α-helices (the N- and the C-helix) are connected by a short loop (Fig. 1A). Furthermore, the protomers dimerize in an antiparallel arrangement, in which the N and C helices of one protomer pack against the N and C helices of the second protomer, forming a four-helix bundle. The two protomers in an asymmetric

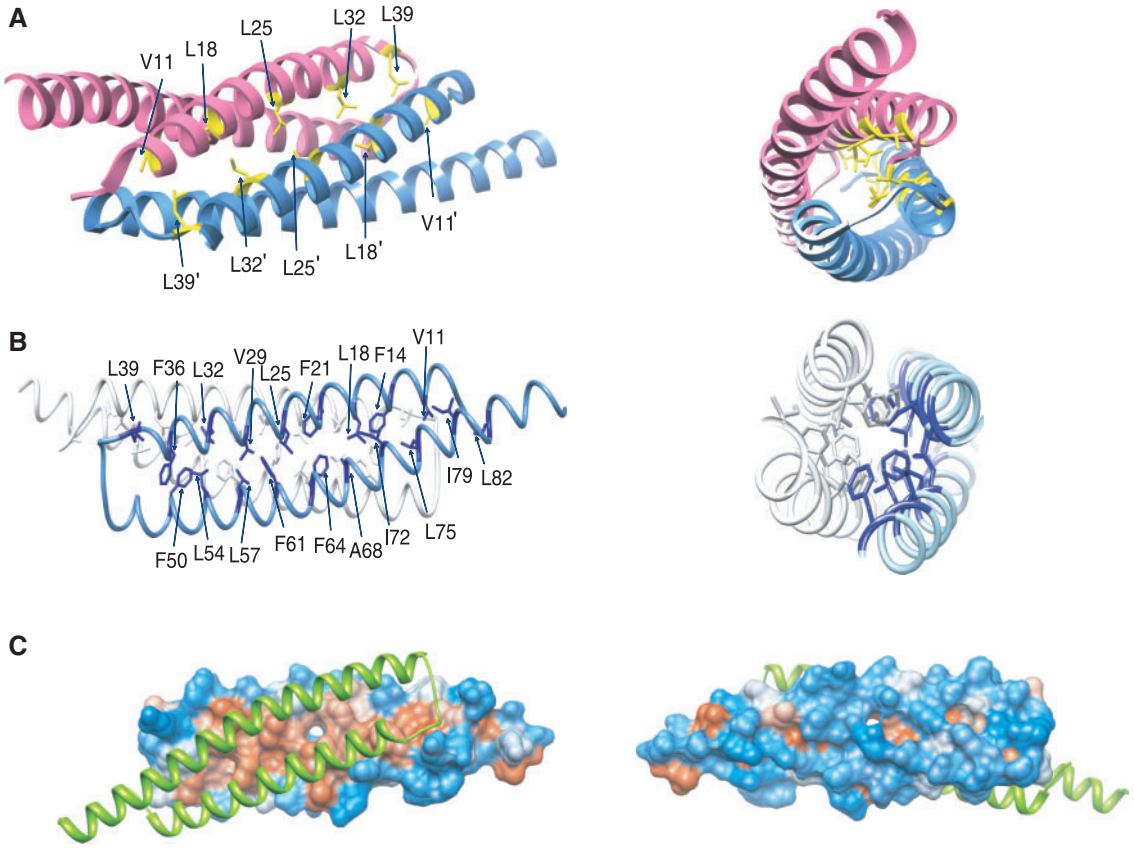

Fig. 1. **Structure of the HP0062 dimer and molecular details of the dimerization interface.** (A) Ribbon diagram of the HP0062 dimer is represented. One monomer is in blue, the other in pink. Side and top views of the HP0062, showing the leucine zipper (yellow). (B) The C_α traces of subunit A (blue) and B (grey) are shown in coil representation, and the interface residues (marked in Fig.3) are shown in ball-and-stick representation. For clarity, only residues of subunit A are labelled. (C) A calculated hydrophobicity of subunit A (red, hydrophobic; blue, hydrophilic; white, neutral), showing the hydrophobic face in the dimerization interface and hydrophilic side in the outer face (rotated 180°). The partner subunit B of the HP0062 dimer is shown in ribbon diagram and coloured in green. The diagrams were generated by UCSF Chimera (*27*).

unit of the orthorhombic crystal are similar, and the topologically equivalent C_α carbons superimpose with a root mean square deviation (RMSD) of 0.79 Å. The overall dimensions of the dimer are about $15 \times 16 \times 67$ Å. We propose that the dimer seen in the crystal is a biologically relevant, since the dimeric state is consistent with the oligomeric form seen by gel filtration chromatography (Fig. 2). Previously, Binkowski *et al*. determined the structure of HP0062 at 2.1 Å in a $P3_121$ space group as a monomer (PDB ID: 2gts). The previous structure is almost identical with this (the topologically equivalent C_α carbons superimpose with a RMSD of 0.58 Å), and also forms a dimer through crystallographic symmetry. So, the overall structure and dimeric state is consistent with the previous report, even though the pH of the crystallization solution is different (7.4 compared with 4.5).

Dimerization Interface and Thermostability—The leucine zipper is a typical member of the coiled coil family, the most common and extensively investigated structural motifs (*12*). The leucine zipper domain is defined as an α-helix comprised of heptad repeats $(abcdefg)_n$, in which

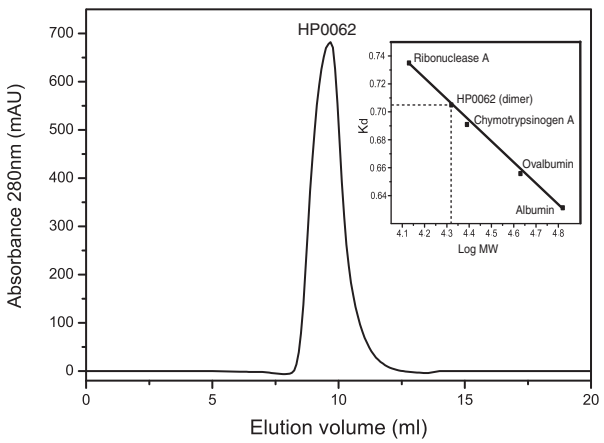

Fig. 2. **Analytical gel filtration of HP0062 at pH 7.5 and 25°C on a BioSep-SEC-S 3000 column.** HP0062 elutes with a retention volume of 9.69 ml, corresponding to the mass of the homodimer. (*Inset*) Calibration of the gel filtration column. The dotted line indicates the logarithm of the apparent molecular mass and K_d of HP0062.

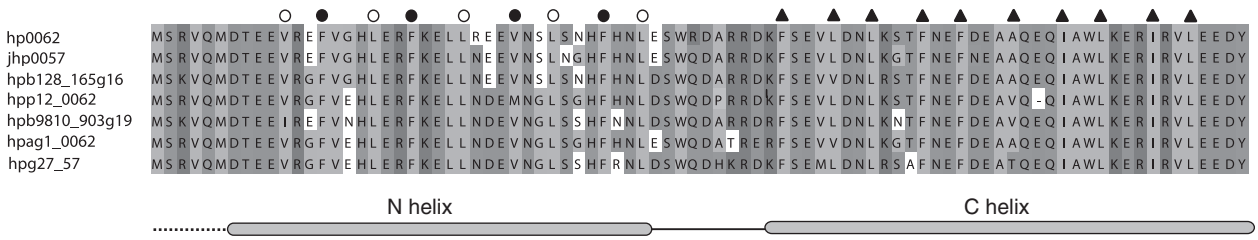

Fig. 3. **Multiple sequence alignment of the HP0062 and its homologues.** HP0062 from *H. pylori* 26695 aligned with the sequences of homologous proteins from *H. pylori* J99 (jhp0057), *H. pylori* B128 (hpb128_165g16), *H. pylori* P12 (hpp12_0062), *H. pylori* 98-10 (hp9810_903g19), *H. pylori* HPAG1 (hpag1_0062) and *H. pylori* g27 (hpg27_57). The secondary structure elements are indicated as black bars (α-helices), black line (coil region) and black dashed line (disordered residues). The participation of various residues in the formation of the dimer interface is indicated by open circles (leucine zipper) and solid circles (aromatic residues) for the N-helix and by solid triangles for the corresponding hydrophobic residues of the C-helix. Sequence alignment was generated by CLUSTAL W (*28*).

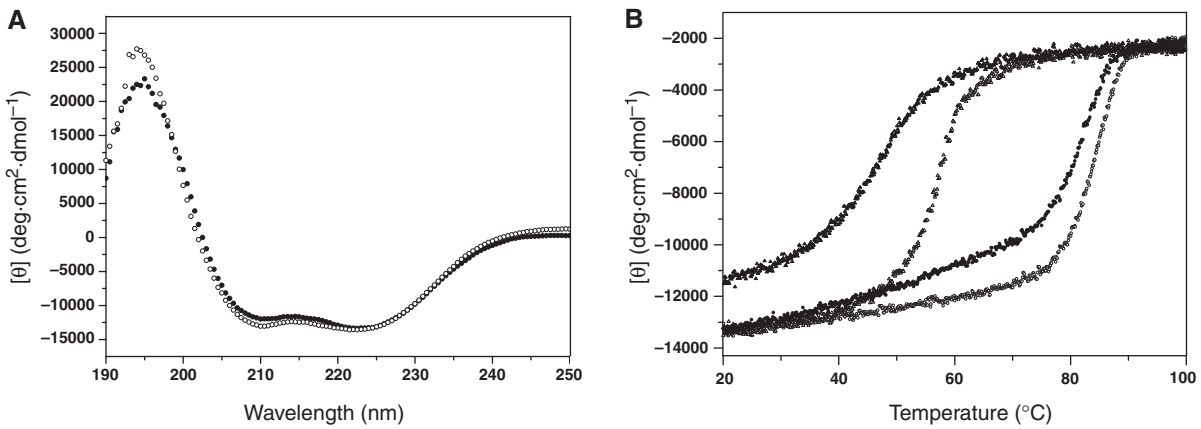

Fig. 4. **Thermal denaturation and renaturation profiles of wild-type and mutant HP0062.** (A) Far-UV CD spectra of wild-type (filled circle) and $HP0062_{F14,21,36A}$ mutant (open circle) are plotted as molar ellipticity versus wavelength. Plots of molar ellipticity versus wavelength in far-UV range of wild-type HP0062 and its mutant are nearly superimposable. (B) Thermal denaturation profiles of wild-type (open circle) and $HP0062_{F14,21,36A}$ mutant (open triangle) and thermal renaturation profiles of wild-type (filled circle) and $HP0062_{F14,21,36A}$ mutant (filled triangle). Changes in molar ellipticity at 222 nm at a scan rate of 1°C/min in the temperature range of 20–100°C were measured. Conditions used for both assays are described under the MATERIALS AND METHODS section.

the residues at positions *a* and *d* are hydrophobic (mainly leucine at position *d*) and mediate critical interhelical interactions, while *b*, *c*, *e*, *f* and *g* are hydrophilic and form the solvent-exposed part of coiled-coil (*13*). Primary structure of HP0062 displays a modified leucine zipper at N-helix, in which additional aromatic residues are located at *a* or *g* position in the leucine zipper, giving the protein stronger hydrophobic interactions. The multiple sequence alignment shown in Fig. 3 reveals that the leucine zipper and additional aromatic residues in N-helix and corresponding hydrophobic residues in C-helix are well conserved. As expected with the sequence analysis, the two protomers in the dimer are primarily held together by hydrophobic interactions (Fig. 1), burying ~1,748 Å^2 of surface area. The leucine, isoleucine, alanine, valine and phenylalanine side chains at positions *a*, *d* and *g* point to the centre of the dimer (Fig. 1A and B). The inner dimerization interface of the monomer shows a concave hydrophobic surface, while the other outer one displays a hydrophilic surface (Fig. 1C). These dimerization interfaces are basically similar to the previous structure (PDB ID: 2gts).

Usually high core/internal hydrophobicity gives the protein high thermostability (*14*). To verify the role of the aromatic residues (F14, F21, F36) in the structural integrity of HP0062, we expressed and purified wild-type and its mutant with triple mutations (F14, 21, 36A). The CD spectrum of the mutant in the far-UV region at 20°C was very similar to that of the wild-type HP0062 (Fig. 4A), indicating that the integrity of the secondary structure of this protein was not affected by the removal of these aromatic residues. We then determined the T_{app} as described previously to compare thermostabilities of HP0062 wild-type and its triple mutant protein. As shown in Fig. 4B, the T_{app} values for the triple mutant was decreased dramatically to 57.0°C (open triangle) compared with that of the wild-type HP0062 (82.8°C, open circle). Moreover, HP0062 wild-type (solid circle) and its triple mutant protein (solid triangle) recovered the folding when the temperature gradually decreased. On the other hand, the triple mutant retained the dimeric state according to gel filtration chromatography (data not shown). These demonstrate that aromatic residues located at *a* or *g* position in the heptad leucine

zipper are not major contributor required for HP0062 dimerization, but important for the thermostability of this protein. It seems that the extensive hydrophobic interactions including leucine zipper is enough for the dimerization.

Structural Comparison and Biological Implication—A search for structural homologues using program DALI (*15*) within the protein data bank shows that the overall structure of HP0062 has similarity with the coiled-coil segments of over 100 functionally unrelated proteins that are involved in various protein–protein interactions. They include among others Rad50 from *Pyrococcus furiosus* (ATPase, PDB code 1l8d, *Z*-score = 8.4, RMSD = 2.2), gp41 from HIV (transmembrane glycoprotein, PDB code 1f23, *Z*-score = 8.2, RMSD = 1.8) and p58/p45 from *Rattus norvegicus* (nucleoporin, PDB code 2osz, *Z*-score = 8.0, RMSD = 3.9). Fold-matched structures identified by the SSM program (*16*) executed by ProFunc Server (*17*) include not only Rad50 from *P. furiosus* (ATPase, PDB code 1l8d, *Q*-score = 0.558, RMSD = 1.71) and gp41 from HIV (transmembrane glycoprotein, PDB code 3cp1, *Q*-score = 0.522, RMSD = 2.09), but also EsxA from *Staphylococcus aureus* (virulence factor, PDB code 2vrz, *Q*-score = 0.612, RMSD = 1.90). EsxA and EsxB are secreted by an ESAT-6-like system that is required for the pathogenesis of *S. aureus* infectons (*18*). The secreted *Mycobacterium tuberculosis* CFP-10 (culture filtrate protein-10 kDa) and ESAT-6 (early secreted antigenic target-6 kDa) complex (1:1 complex) have been shown to play an essential role in tuberculosis pathogenesis (*19*). Structures of *S. aureus* EsxA dimer (*20*) and *M. tuberculosis* CFP-10/ESAT-6 complex (*21*) have recently been determined. Despite the very low sequence conservation (*S. aureus* EsxA shares 12% sequence identity with ESAT-6, 14% with CFP-10 and 13% with *S. aureus* EsxB), the structures are similar. They share a similar helix–hairpin–helix topology with the HP0062 dimer, despite no sequence similarity with HP0062 at all.

The ESAT-6/WXG100 superfamily, observed in many Gram-positive bacteria including *M. tuberculosis, Bacillus subtilis, B. anthracis, S. aureus* and *Clostridium acetobutylicum*, is composed of approximately 100 amino acids, exists as gene clusters, is exported from the cell with no signal peptides but with a Trp-X-Gly signature motif, and possesses extensive coiled-coil domains (*22*). These family proteins are speculated as a new Gram-positive secretion system potentially driven by the FtsK/SpoIIIE ATPase domains in the YukA-like proteins (*22*). Interestingly, the HP0062 orthologues are found in similar neighbourhoods in all known genomes of *H. pyori* strains (data not shown). The most common neighbour of HP0062 in these genomes is a conserved hypothetical ATP-binding protein [HP0066 in the case of *H. plylori* 26695], which has a FtsK/SpoIIIE domain when analysed by PFAM (http://www.sanger.ac.uk/Pfam).

On the other hand, a number of Gram-negative animal and plant pathogenic bacteria use type III secretion (TTS) systems to target bacterial effector proteins into eukaryotic cells. This system requires more than 20 proteins and its core components are homologous to proteins essential for the assembly of surface flagella required for bacterial motility (*23–25*). TTS chaperones are found in almost all bacteria that use flagellar and/or virulence-associated TTS systems. These chaperones share common features, including small (12–18 kDa) dimer, an acidic pI, an overall α-helical character and a putative carboxy-terminal amphipathic helix that is thought to mediate interactions with their cognate substrate proteins (*23*, *24*). The structure of one such chaperone, FliS, reveals a compact four-helix bundle that binds its target protein in an extended conformation (*26*).

Surprisingly, HP0062 shows extensively similar characteristics to those of the ESAT-6 family of Gram-positive bacteria; small dimer, helix–hairpin–helix structure, no signal peptide but with WXG motif in the hairpin bend (WRD in HP0062), and gene clusters with a protein with FtsK/SpoIIIE domain. And it also has similar characteristics to those of the TTS chaperones of Gram-negative bacteria; small dimer, an acidic pI, an overall α-helical character and a carboxy-terminal amphipathic helix. Taken all together, we speculate that HP0062 might be an ESAT-6 family analogue of *H. pylori* and function as a transport chaperone and/or adaptor protein to facilitate interactions with host receptor proteins. Additional biochemical and biophysical studies including localization experiment and protein–protein interactions with ATP-binding protein could provide valuable insights into the precise function of this protein.

ACKNOWLEDGEMENTS

We thank the staff members of beamline BL-6C of PLS for helpful discussions and technical assistance during X-ray experiments and Dr Hoo-Kang Im for the critical comments on the manuscript.

FUNDING

Ministry of Education, Science and Technology (MEST); Innovative Drug Research Center for Metabolic and Inflammatory Disease; 2008 BK21 Project for Medicine, Dentistry and Pharmacy; New Drug Target Discovery (grant number 370C-20070095).

CONFLICT OF INTEREST

None declared.

REFERENCES

1. Marshall, B.J. and Warren, J.R. (1984) Unidentified curved bacilli in the stomach of patients with gastritis and peptic ulceration. *Lancet* **1**, 1311–1315
2. Peek, R.M. Jr. and Blaser, M.J. (2002) *Helicobacter pylori* and gastrointestinal tract adenocarcinomas. *Nat. Rev.* **2**, 28–37
3. Tomb, J.F., White, O., Kerlavage, A.R., Clayton, R.A., Sutton, G.G., Fleischmann, R.D., Ketchum, K.A., Klenk, H.P., Gill, S., Dougherty, B.A., Nelson, K., Quackenbush, J., Zhou, L., Kirkness, E.F., Peterson, S., Loftus, B., Richardson, D., Dodson, R., Khalak, H.G., Glodek, A., McKenney, K., Fitzegerald, L.M., Lee, N., Adams, M.D., Hickey, E.K., Berg, D.E., Gocayne, J.D., Utterback, T.R., Peterson, J.D., Kelley, J.M., Cotton, M.D., Weidman, J.M., Fujii, C., Bowman, C., Watthey, L.,

Wallin, E., Hayes, W.S., Borodovsky, M., Karp, P.D., Smith, H.O., Fraser, C.M., and Venter, J.C. (1997) The complete genome sequence of the gastric pathogen *Helicobacter pylori*. *Nature* **388**, 539–547
4. Alm, R.A., Ling, L.S., Moir, D.T., King, B.L., Brown, E.D., Doig, P.C., Smith, D.R., Noonan, B., Guild, B.C., deJonge, B.L., Carmel, G., Tummino, P.J., Caruso, A., Uria-Nickelsen, M., Mills, D.M., Ives, C., Gibson, R., Merberg, D., Mills, S.D., Jiang, Q., Taylor, D.E., Vovis, G.F., and Trust, T.J. (1999) Genomic-sequence comparison of two unrelated isolates of the human gastric pathogen *Helicobacter pylori*. *Nature* **397**, 176–180
5. Oh, J.D., Kling-Backhed, H., Giannakis, M., Xu, J., Fulton, R.S., Fulton, L.A., Cordum, H.S., Wang, C., Elliott, G., Edwards, J., Mardis, E.R., Engstrand, L.G., and Gordon, J.I. (2006) The complete genome sequence of a chronic atrophic gastritis *Helicobacter pylori* strain: evolution during disease progression. *Proc. Natl Acad. Sci. USA* **103**, 9999–10004
6. (1994) The CCP4 suite: programs for protein crystallography. *Acta Crystallogr. D Biol. Crystallogr*. **50**, 760–763
7. Navaza, J. (2001) Implementation of molecular replacement in AMoRe. *Acta Crystallogr. D Biol. Crystallogr.* **57**, 1367–1372
8. Emsley, P. and Cowtan, K. (2004) Coot: model-building tools for molecular graphics. *Acta Crystallogr. D Biol. Crystallogr.* **60**, 2126–2132
9. Brunger, A.T., Adams, P.D., Clore, G.M., Delano, W.L., Gros, P., Grosse-Kunstleve, R.W., Jiang, J.S., Kuszewski, J., Nilges, M., Pannu, N.S., Read, R.J., Rice, L.M., Simonson, T., and Warren, G.L. (1998) Crystallography & NMR system: a new software suite for macromolecular structure determination. *Acta Crystallogr. D Biol. Crystallogr.* **54**, 905–921
10. Murshudov, G.N., Vagin, A.A., and Dodson, E.J. (1997) Refinement of macromolecular structures by the maximum-likelihood method. *Acta Crystallogr. D Biol. Crystallogr.* **53**, 240–255
11. Winn, M.D., Murshudov, G.N., and Papiz, M.Z. (2003) Macromolecular TLS refinement in REFMAC at moderate resolutions. *Methods Enzymol.* **374**, 300–321
12. Lupas, A. (1996) Coiled coils: new structures and new functions. *Trends Biochem. Sci.* **21**, 375–382
13. Cohen, C. and Parry, D.A. (1990) Alpha-helical coiled coils and bundles: how to design an alpha-helical protein. *Proteins* **7**, 1–15
14. Schumann, J., Bohm, G., Schumacher, G., Rudolph, R., and Jaenicke, R. (1993) Stabilization of creatinase from Pseudomonas putida by random mutagenesis. *Protein Sci.* **2**, 1612–1620
15. Holm, L. and Sander, C. (1995) Dali: a network tool for protein structure comparison. *Trends Biochem. Sci.* **20**, 478–480
16. Krissinel, E. and Henrick, K. (2004) Secondary-structure matching (SSM), a new tool for fast protein structure alignment in three dimensions. *Acta Crystallogr. D Biol. Crystallogr.* **60**, 2256–2268
17. Laskowski, R.A., Watson, J.D., and Thornton, J.M. (2005) ProFunc: a server for predicting protein function from 3D structure. *Nucleic Acids Res.* **33**, W89–W93
18. Burts, M.L., Williams, W.A., Debord, K., and Missiakas, D.M. (2005) EsxA and EsxB are secreted by an ESAT-6-like system that is required for the pathogenesis of Staphylococcus aureus infections. *Proc. Natl Acad. Sci. USA* **102**, 1169–1174
19. Stanley, S.A., Raghavan, S., Hwang, W.W., and Cox, J.S. (2003) Acute infection and macrophage subversion by Mycobacterium tuberculosis require a specialized secretion system. *Proc. Natl Acad. Sci. USA* **100**, 13001–13006
20. Sundaramoorthy, R., Fyfe, P.K., and Hunter, W.N. (2008) Structure of Staphylococcus aureus EsxA suggests a contribution to virulence by action as a transport chaperone and/or adaptor protein. *J. Mol. Biol.* **383**, 603–614
21. Renshaw, P.S., Lightbody, K.L., Veverka, V., Muskett, F.W., Kelly, G., Frenkiel, T.A., Gordon, S.V., Hewinson, R.G., Burke, B., Norman, J., Williamson, R.A., and Carr, M.D. (2005) Structure and function of the complex formed by the tuberculosis virulence factors CFP-10 and ESAT-6. *EMBO J.* **24**, 2491–2498
22. Pallen, M.J. (2002) The ESAT-6/WXG100 superfamily – and a new Gram-positive secretion system? *Trends Microbiol.* **10**, 209–212
23. Bennett, J.C. and Hughes, C. (2000) From flagellum assembly to virulence: the extended family of type III export chaperones. *Trends Microbiol.* **8**, 202–204
24. Plano, G.V., Day, J.B., and Ferracci, F. (2001) Type III export: new uses for an old pathway. *Mol. Microbiol.* **40**, 284–293
25. Cheng, L.W. and Schneewind, O. (2000) Type III machines of Gram-negative bacteria: delivering the goods. *Trends Microbiol.* **8**, 214–220
26. Evdokimov, A.G., Phan, J., Tropea, J.E., Routzahn, K.M., Peters, H.K., Pokross, M., and Waugh, D.S. (2003) Similar modes of polypeptide recognition by export chaperones in flagellar biosynthesis and type III secretion. *Nat. Struct. Biol.* **10**, 789–793
27. Pettersen, E.F., Goddard, T.D., Huang, C.C., Couch, G.S., Greenblatt, D.M., Meng, E.C., and Ferrin, T.E. (2004) UCSF Chimera–a visualization system for exploratory research and analysis. *J. Comput. Chem.* **25**, 1605–1612
28. Thompson, J.D., Higgins, D.G., and Gibson, T.J. (1994) CLUSTAL W: improving the sensitivity of progressive multiple sequence alignment through sequence weighting, position-specific gap penalties and weight matrix choice. *Nucleic Acids Res.* **22**, 4673–4680